ARTICLES
PUBLISHED ONLINE: 4 JULY 2016 | DOI: 10.1038/NMAT4686
nature materials

Topological edge states in a high-temperature superconductor FeSe/$SrTiO_3$(001) film

Z. F. Wang[1,2,3†], Huimin Zhang[2,4†], Defa Liu[5], Chong Liu[2], Chenjia Tang[2], Canli Song[2], Yong Zhong[2], Junping Peng[2,4], Fangsen Li[2], Caina Nie[2,4], Lili Wang[2,6], X. J. Zhou[5,6*], Xucun Ma[2,4,6*], Q. K. Xue[2,6] and Feng Liu[2,3,6*]

Superconducting and topological states are two most intriguing quantum phenomena in solid materials. The entanglement of these two states, the topological superconducting state, will give rise to even more exotic quantum phenomena. While many materials are found to be either a superconductor or a topological insulator, it is very rare that both states exist in one material. Here, we demonstrate by first-principles theory as well as scanning tunnelling spectroscopy and angle-resolved photoemission spectroscopy experiments that the recently discovered 'two-dimensional (2D) superconductor' of single-layer FeSe also exhibits 1D topological edge states within an energy gap of ∼40 meV at the M point below the Fermi level. It is the first 2D material that supports both superconducting and topological states, offering an exciting opportunity to study 2D topological superconductors through the proximity effect.

High-quality single-layer FeSe thin film has been successfully grown on the $SrTiO_3$(001) (STO) substrate[1] (see Methods for more details). A large superconducting gap, with a transition temperature (T_c) as high as ∼40–100 K (refs 1–7), is measured by different experimental techniques. Despite intensive efforts, some fundamental properties of this interesting new class of '2D superconductor' remain unclear. One outstanding inconsistency between experiment and theory lies in its band structure. In the superconducting phase, angle-resolved photoemission spectroscopy (ARPES) experiments[2–5] have shown that the Fermi surface of single-layer FeSe/STO is characterized by only electron pockets at the M point but no hole pockets at the Γ point. Furthermore, there is an energy gap of ∼40 meV below the Fermi level at the M point. However, these key features have not been reproduced by theory consistently.

Recently, the possible existence of topological phases in FeSe has drawn much attention[8–10]. In this work, we demonstrate both theoretical and experimental evidence for an antiferromagnetic (AFM) quantum spin Hall (QSH) state in FeSe. First, we determined the most plausible magnetic state of the experimental sample. Currently, there are no direct experimental spin-polarized scanning tunnelling microscopy (STM) or neutron scattering data to pin down the magnetic state of FeSe/STO. On the other hand, the present state-of-the-art first-principles methods are not able to reliably predict the magnetic ground state of FeSe/STO (ref. 11). Thus, to solve the problem, alternatively we took an indirect approach by calculating the band structure of FeSe/STO in non-magnetic and different possible magnetic configurations (Supplementary Figs 1–4) to match the experimental ARPES data. We found that only the band structure in the chequerboard AFM configuration with spin along the z direction can give a good agreement. Next, focusing on the chequerboard AFM state of FeSe/STO, we have extended previous theoretical studies[11–15] to include the spin–orbital coupling (SOC) effect. We found that not only a gap is opened by SOC (Supplementary Fig. 5) at the right position (in both energy and reciprocal space) with a gap size comparable to the experimental value (∼40 meV), but also the band structure within the whole Brillouin zone is consistent with the ARPES measurement. Most remarkably, a 1D topological edge state (AFM QSH state), which is revealed to be associated with this SOC gap, is confirmed by scanning tunnelling spectroscopy (STS) measurement in both energy and real space. In contrast to studies demonstrating extrinsic doping-induced superconductor phases in Cu-doped Bi_2Se_3 (ref. 16) and In-doped SnTe (ref. 17), our work demonstrates an intrinsic topological phase in Fe-based superconductors that was unknown before, offering an exciting opportunity to study the topological and superconducting states in one single material.

As a benchmark, we first repeated the previous calculations without SOC (see Methods for more details). The interface structure of FeSe/STO is complex in the experimental sample (Supplementary Fig. 6); one possible atomic structure of FeSe/STO is shown in Fig. 1a (an alternative structure is shown in Supplementary Fig. 7 and produces qualitatively similar results). In our calculations, we assume that the bottom Se atom in single-layer FeSe is directly above the top Ti atom in the STO substrate at a calculated distance of ∼3 Å. The spin configuration of the chequerboard AFM state (neighbouring Fe atoms have opposite spin directions) is schematically shown in Fig. 1b, and the calculated magnetic moment of ∼2.3μ_B along the z direction is localized on Fe atoms. The corresponding spin-polarized band structures with Hubbard-U correction show that except a small band splitting along the X–M–X′ direction, the spin-up (red) and spin-down (blue) bands are almost degenerate (Supplementary Fig. 8a). One sees that there are only

[1]Hefei National Laboratory for Physical Sciences at the Microscale, Synergetic Innovation Center of Quantum Information and Quantum Physics, University of Science and Technology of China, Hefei, Anhui 230026, China. [2]State Key Lab of Low-Dimensional Quantum Physics, Department of Physics, Tsinghua University, Beijing 100084, China. [3]Department of Materials Science and Engineering, University of Utah, Utah 84112, USA. [4]Institute of Physics, Chinese Academy of Sciences, Beijing 100190, China. [5]National Lab for Superconductivity, Beijing National Laboratory for Condensed Matter Physics, Institute of Physics, Chinese Academy of Sciences, Beijing 100190, China. [6]Collaborative Innovation Center of Quantum Matter, Beijing 100084, China. †These authors contributed equally to this work. *e-mail: XJZhou@aphy.iphy.ac.cn; xucunma@mail.tsinghua.edu.cn; fliu@eng.utah.edu

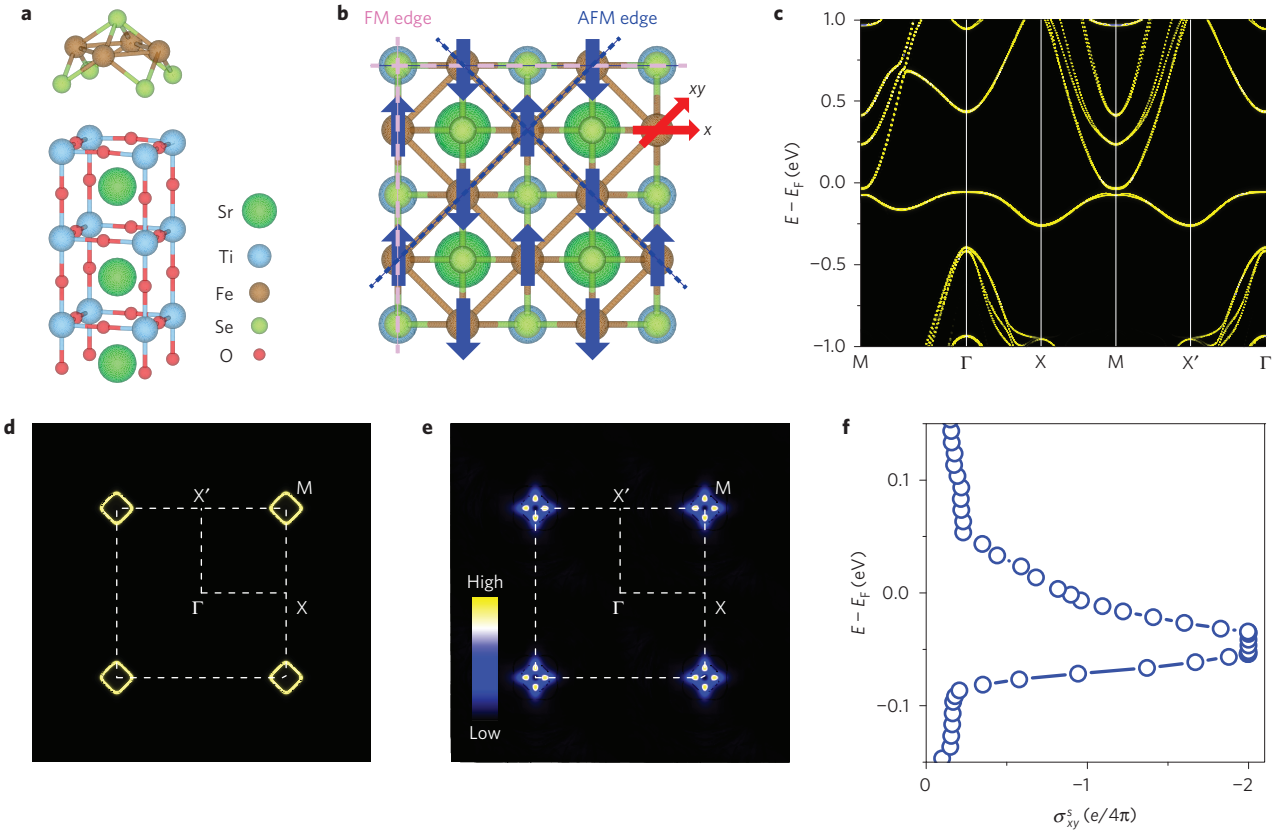

Figure 1 | Theoretical atomic structure, band structure and quantized spin Hall conductance. a, One possible atomic structure of single-layer FeSe on the TiO_2-terminated $SrTiO_3$(001) surface. **b**, Chequerboard AFM spin configuration of Fe atoms. The blue arrows denote spin-up and spin-down along the *z* direction. The spin along the in-plane *xy* and *x* directions is denoted by red arrows. Two different FM and AFM edges are highlighted by the dashed and dotted lines with different colours, respectively. **c**, Projected band structures with SOC onto the single-layer FeSe. **d**, Fermi surface of the band structures shown in **c**. **e**, Reciprocal-space distribution of spin Berry curvature within the SOC gap. **f**, Spin Hall conductance as a function of the Fermi level, showing a quantized value within the energy window of the SOC gap.

electron pockets at the M point but no hole pocket at the Γ point, consistent with the ARPES data[2–5] and previous calculations[14,15]. We also checked orbital components around the Fermi level. The extended flat bands below the Fermi level, which are sensitive to the Hubbard-U correction (Supplementary Figs 9–11), originate mainly from the d_z^2, d_{xz} and d_{yz} orbitals of the Fe atoms, and the p_z orbital of the Se atoms.

However, the bandgap at the M point below the Fermi level as observed in ARPES is absent in the above calculations (Supplementary Fig. 8a). Next, we consider the SOC effect in FeSe/STO (Supplementary Fig. 8b). The most important finding is that a SOC gap, with a value of ∼33 meV, is opened at the M point below the Fermi level, in very good agreement with the experiment. In the calculation, the spin direction on Fe atoms is set along the *z* axis, as the in-plane spin configuration cannot open a sizeable gap at the M point (see Supplementary Fig. 5). To clearly see the contributions of FeSe on the whole bands, we projected the total bands onto single-layer FeSe, as shown in Fig. 1c. Comparing Fig. 1c and Supplementary Fig. 8b, we found that the hybridization between FeSe and STO substrate is negligible, and the parabolic bands overlapping with the FeSe bands around the M point come completely from the STO substrate. Thus, the effect of the STO substrate is only to introduce electron doping in FeSe, as the Fermi level passes through the band crossing points between FeSe and STO. This is also confirmed by our calculations of free-standing single-layer FeSe, in which the Fermi level is inside the SOC gap (Supplementary Fig. 5). The corresponding Fermi surface of the bands in Fig. 1c is plotted in Fig. 1d, showing only electron pockets around four M points.

To further support our first-principles band-structure results, we have extended previous ARPES experiments[2–5] by measuring the band structure of FeSe/STO along different high-symmetry directions in the Brillouin zone, as defined in Fig. 2a (see Methods for more details). The first-principles bands are overlaid with the second-derivative ARPES spectra around Γ (M) points in Fig. 2b (2c) and along other high-symmetry directions in Fig. 2d–f, respectively (the raw ARPES spectrum is shown in Supplementary Fig. 12). One sees that the agreement between the calculated bands and the ARPES spectra is very good, not only around Γ and M points but also in the whole Brillouin zone (to match ARPES spectra, the Fermi level of first-principles bands is slightly shifted upward, using the SOC gap at the M point as a reference). We note that by including SOC, our first-principles bands reproduced all critical salient features observed experimentally. Furthermore, to clearly illustrate the M point bandgap below the Fermi level, we have also measured the ARPES spectra along the perpendicular direction of cut no. 2 in Fig. 2a (Supplementary Fig. 13). The M point bandgap can be observed along this perpendicular direction too, demonstrating that the gap is a global gap, consistent with our calculated band structures. Thus, by matching the first-principles bands for different spin configurations to the experimental ARPES, we determine that the FeSe/STO has a chequerboard AFM state. The existence of an AFM phase might bear some relationship with the superconducting phase. For example, many-body electron–electron and electron–phonon interactions, as well as doping and interfacial effects, might suppress the AFM ordering in favour of the superconducting ordering. These interesting questions deserve

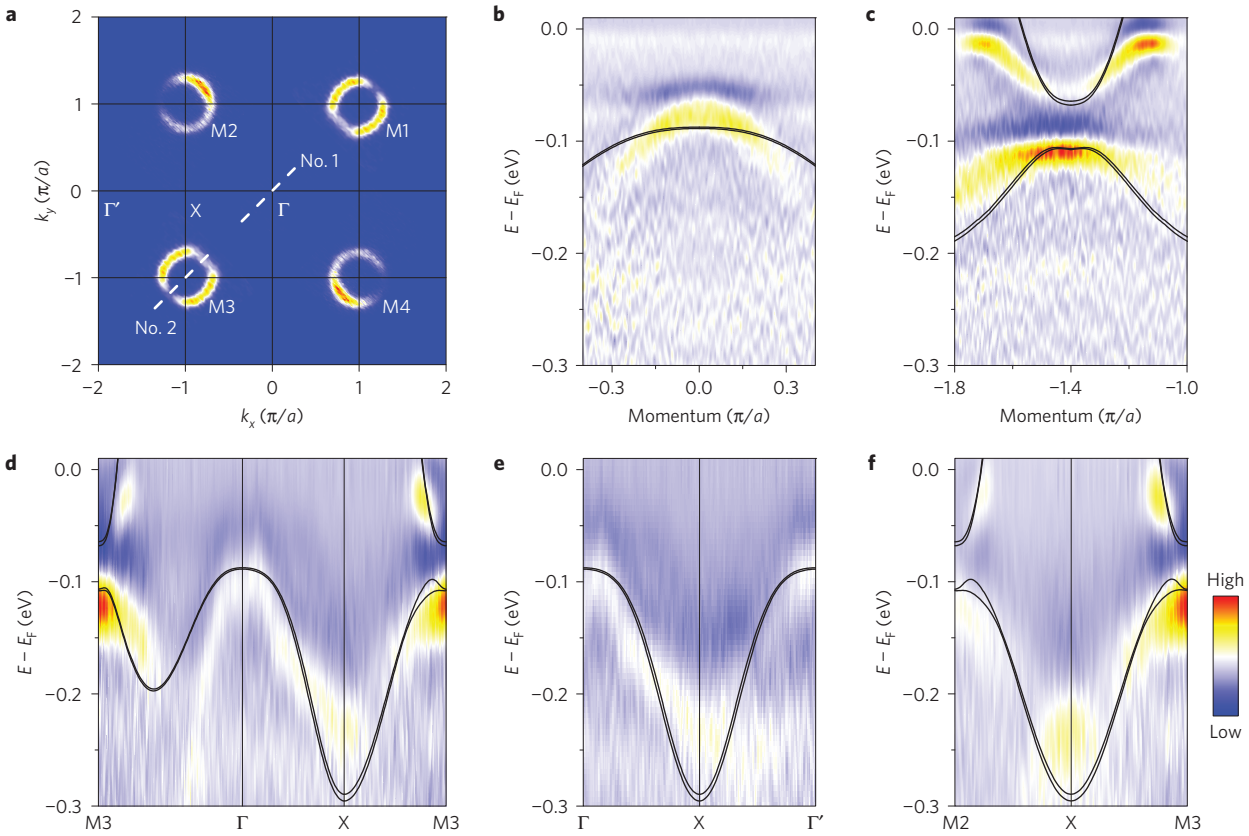

Figure 2 | Band-structure comparison between theory and second-derivative ARPES spectra. a, Experimental ARPES Fermi surface and high-symmetry k points of FeSe/STO. The spectral intensity is obtained by integrating over an energy window (−0.01 eV, 0.01 eV) around the Fermi level. **b**,**c**, Theoretical band structures of FeSe/STO overlapped with experimental second-derivative ARPES spectra around the Γ (cut no. 1 in **a**) and M (cut no. 2 in **a**) points, respectively. **d**–**f**, Theoretical band structures of FeSe/STO overlapped with experimental second-derivative ARPES spectra along different high-symmetry directions. The black lines in **b**–**f** are theoretical band structures.

further many-body theoretical studies much beyond the single-particle picture given by the first-principles calculations. Here, instead, we will focus on a possible topological phase ordering associated with the SOC gap in the AFM state, which can be reliably predicted from first principles.

Generally, the bandgap opened by SOC is non-trivial, such as in the case of 2D topological insulators[18]. To check the topology of this SOC gap in FeSe/STO, the spin Chern number (C_s) and spin Hall conductance (σ^s_{xy}) of FeSe/STO are calculated using the standard Kubo formula[19]. The reciprocal-space distribution of spin Berry curvature for the Fermi level within the SOC gap is shown in Fig. 1e, which is non-zero around four M points. Integration of spin Berry curvature gives an integer value $C_s = -1$. Figure 1f shows the calculated spin Hall conductance as a function of Fermi level, which shows a quantized value within the energy window of the SOC gap, indicating an AFM QSH state. We also constructed a tight-binding model Hamiltonian to understand the SOC mechanism in FeSe/STO, and found that the SOC gap at the M point is opened by an on-site coupling between the d_{xz} and d_{yz} orbitals of the Fe atoms (Supplementary Fig. 14).

Different from the conventional QSH state[20,21], the time-reversal symmetry is broken in the AFM QSH state. However, the combined symmetry of time-reversal and primitive-lattice-translation is preserved, which has been used to study 3D AFM topological insulators[22,23]. On the basis of the Bernevig–Hughes–Zhang model with an AFM stagger potential, it has been shown[24] that although the non-magnetic disorder can break this combined symmetry, the edge states in the AFM QSH state are still robust against non-magnetic disorder if spin-up and spin-down channels are decoupled from each other. This is really the case here because of the integer spin Chern number, so that s_z can be effectively considered as a good quantum number in FeSe/STO.

As a further confirmation of the spin Chern number calculation, 1D edge states of a FeSe/STO ribbon with both FM and AFM edges (as illustrated in Fig. 1b) are calculated using the Wannier functions[25–27]. For the FM edge ribbon (Fig. 3a), there are two asymmetric edge states inside the SOC gap for both the left and right edges (the spin symmetry is broken along the FM edge), as shown in Fig. 3b, and the edge and bulk state projected bands can be further clearly distinguished in Fig. 3c–e. The left and right edge states have the same dispersion (both edges are terminated with Fe and Se atoms), but slightly split. The Dirac point (denoted by the arrow in Fig. 3b) is not at high symmetry k point. For the AFM edge ribbon (Fig. 3f), the edge states become symmetric (the spin symmetry is preserved along the AFM edge), and their shapes on the left (terminated with Fe and Se atoms) and right (terminated with only Se atom) edges are dramatically different from each other, as shown in Fig. 3g–j. The Dirac points (denoted by the arrows in Fig. 3g) are at high-symmetry k points (Brillouin zone centre or boundary). Most importantly, inside the SOC gap, we can see that the valence and conduction bulk bands are connected with a pair of gapless Dirac edge states for both the FM and AFM edges, demonstrating the characteristic feature of the AFM QSH state, which is also consistent with the theoretical model prediction in ref. 24.

Finally, we present experimental evidence for the existence of 1D topological edge states. We have carried out systematically STS measurement of the edge state of FeSe/STO (see Methods for more

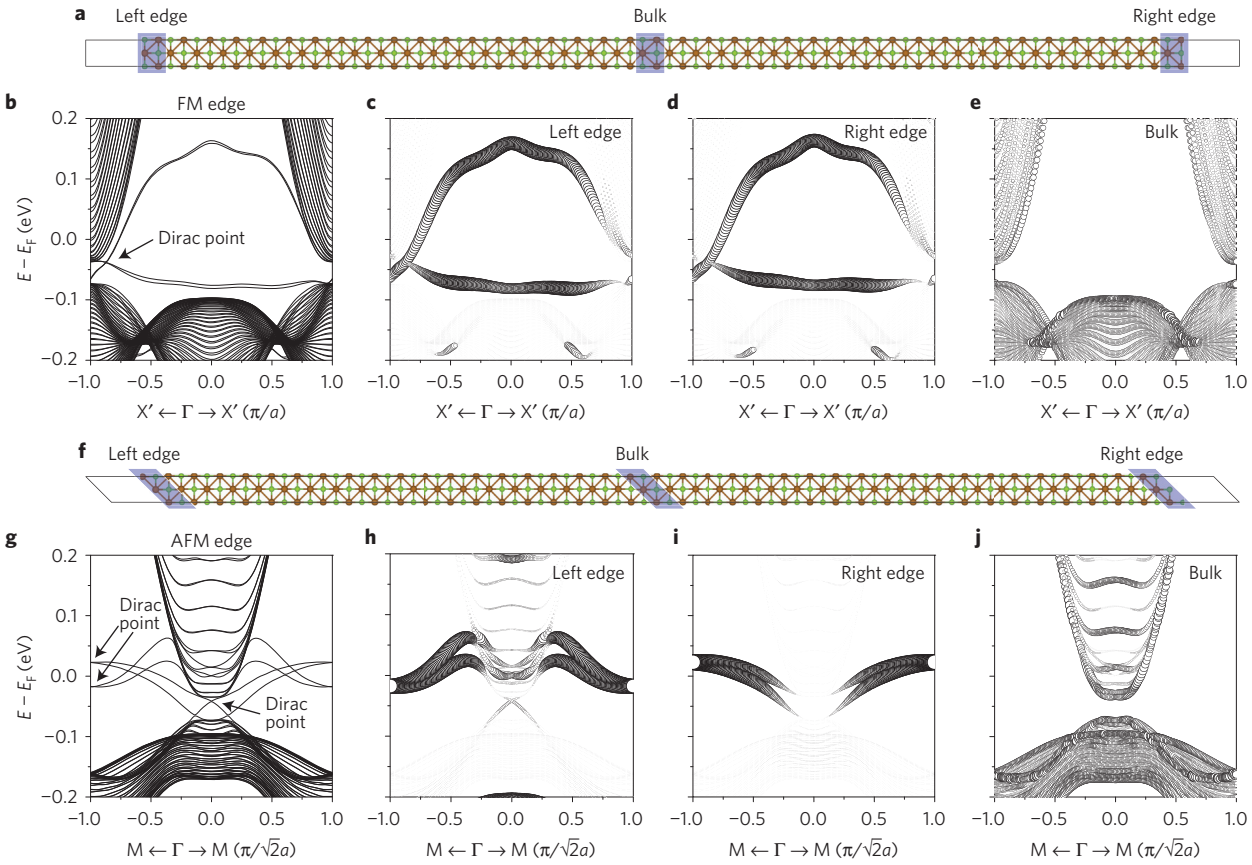

Figure 3 | Theoretical topological edge state of FeSe/STO. a, Atomic structure of a 1D FeSe/STO ribbon for the FM edge. **b**, 1D band structure for **a**. **c**–**e**, 1D band structure projected onto the left edge, right edge and bulk of one unit cell for **a**, showing the left edge state, right edge state and bulk state, respectively. **f**–**j**, The same as **a**–**e**, but for the AFM edge. In all projected bands, the circle size denotes the weighting factor of the corresponding states.

details). The STS edge state measurements are taken along two different edges: FM (Fig. 4a and Supplementary Fig. 15) and AFM edges (Fig. 4b). The atomic-resolution topographies taken near the edge, showing the bulk Se atom arrangement, are shown in the insets of Fig. 4a,b. Since the film is continuous from bulk to edge, on the basis of the bulk Se atom arrangement, we are able to determine the orientations of these two edges: FM and AFM edges are along the [100] and [1$\bar{1}$0] directions, respectively. The corresponding line scans of STS spectra at the marked positions along the blue arrow direction (labelled in Fig. 4a,b) are shown in Fig. 4c,d, respectively. One significant feature has been observed in the spectra, namely, the spectral intensity becomes noticeably larger around −0.1 eV for the FM edge and −0.05 eV for the AFM edge, respectively, when the line scans approach the film edge, indicating the existence of an edge state in FeSe/STO. Furthermore, a 2D STS mapping for the FM edge in Fig. 4a has been performed and one can clearly see the edge state having a width of ∼1 nm in real space (Supplementary Fig. 16). The superconducting gap has also been confirmed at the edge of FeSe/STO, although its magnitude decreases progressively when approaching the edge (Supplementary Fig. 17).

One effective way to reveal the topological origin of the observed edge state in real space is to make a comparison between the real-space STS and the reciprocal-space ARPES spectra in energy space[28]. First, we have compared the superconducting gap of FeSe/STO obtained from dI/dV spectra of STS and the symmetrized energy distribution curve of ARPES in Fig. 4e. By aligning the Fermi level of these two data together (the vertical dashed lines are used to indicate the Fermi level and the edges of superconducting gap), we found that the superconducting gap (∼10 meV) is the same in these two independent measurements. Such a good agreement between STS and ARPES data facilitates reliably the following comparison of edge states. By setting the Fermi level as the reference energy, ARPES and 2D theoretical bands around the M point (Fig. 4f), theoretical bands for the FM edge (Fig. 4g, left panel) and the AFM edge (Fig. 4g, right panel), theoretical local density of states (LDOS) for the FM edge (Fig. 4h, left panel) and the AFM edge (Fig. 4h, right panel) (see also Supplementary Fig. 18) are all aligned with the STS spectra for the FM edge (Fig. 4i, left panel) and the AFM edge (Fig. 4i, right panel), with the region of the SOC gap indicated by a light blue band in Fig. 4f–i. By the principle of bulk-boundary correspondence, the topological edge state differs dramatically from the normal chemical edge states: the former, originating from the bulk Bloch wavefunction, shows an extended DOS and appears at a well-defined energy range across the whole bulk SOC gap depending on where the edge states connect with the bulk band edges; while the latter, originating from a surface wavefunction such as a dangling bond, shows a localized DOS and may appear at an a priori unknown energy. The above-mentioned key topological edge state features can be seen directly in the experimental STS spectra of FM and AFM edges (Fig. 4i) with their different peak positions appearing in the expected energy range, signifying their topological origin in accordance with theoretical predictions (Fig. 4g,h). Furthermore, the shape and overall tendency of experimental STS spectra (Fig. 4i) of both FM and AFM edges versus bulk can be qualitatively reproduced by theoretical LDOS (Fig. 4h, see also Supplementary Fig. 18). Specifically, due to different band dispersions of FM and AFM edge states, they connect with the bulk band edges very differently (Fig. 4g), so that their STS spectra have a dramatically different shape. For the FM (AFM) edge, the maximum difference between the calculated edge and bulk DOS

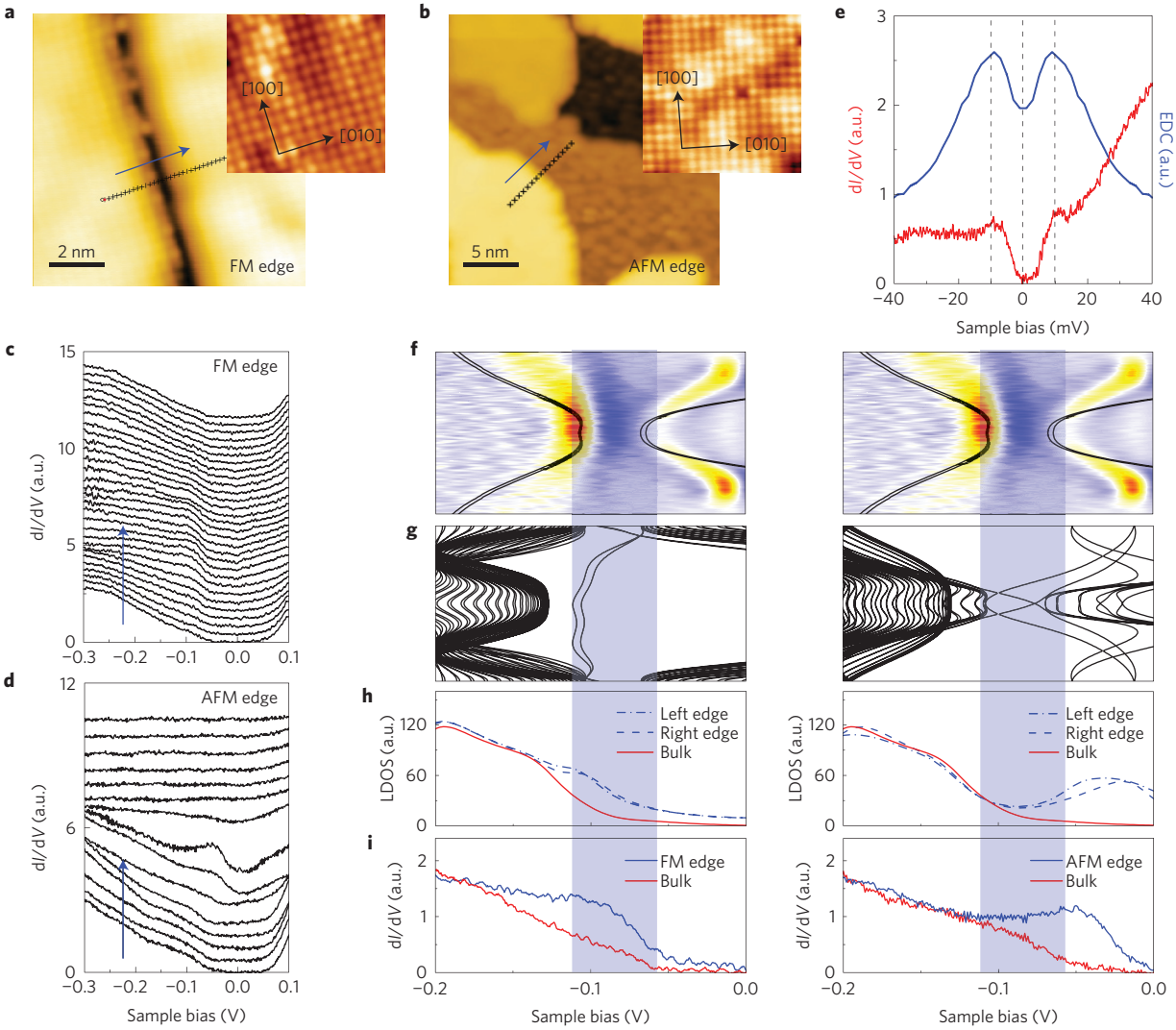

Figure 4 | Topological edge state comparison between theory and STS spectra. a,**b**, Experimental STM topography of the FM edge (0.1 nA, −300 mV) and the AFM edge (0.05 nA, 1 V) of FeSe/STO. The inset shows an atomic-resolution STM topography image at the bulk position of the FM edge (0.1 nA, 100 mV) and the AFM edge (0.1 nA, 100 mV), showing the topmost Se atom arrangement (the crystal orientations are labelled). **c**,**d**, Experimental STS line scanning at the marked positions along the blue arrow direction for the FM edge (0.1 nA, 100 mV) and the AFM edge (0.2 nA, 500 mV) in **a** and **b**. The blue arrows in **c** and **d** indicate the STS line scan direction. **e**, Superconducting gap comparison between experimental d*I*/d*V* spectra (0.1 nA, 50 mV) and the symmetrized energy distribution curve (EDC). **f**, Theoretical and ARPES band structure around the M point. The black lines are theoretical band structures. **g**, Theoretical 1D band structure of a FeSe/STO ribbon with FM (left panel) and AFM (right panel) edges. **h**, Theoretical local density of states (LDOS) for edge and bulk states in **g**. **i**, Experimental STS spectra of edge and bulk states extracted from **c** and **d** for FM (left panel) and AFM (right panel) edges. The light blue band in **f**–**i** indicates the SOC gap.

is within (above) the SOC gap (Fig. 4h). This difference is indeed observed in experiments (Fig. 4i). Therefore, our STS experiments provide confirmation of the 1D topological edge states in FeSe/STO as theoretically predicted.

We note that it has been shown for bulk FeSeTe systems[29,30] that due to a correlation effect, orbital- or band-dependent renormalization should be applied to density functional theory band structures. Similar renormalization effect should also modify the band structures of single-layer FeSe we calculated here for both non-trivial and trivial gap states in comparison with experiments, which calls for future theoretical studies such as dynamic mean field theory calculations. On the other hand, the comparison between theoretical and experimental edge states qualitatively confirms the likelihood of their topological origin-based bulk-boundary correspondence, even though it is quantitatively not perfect, such as too large a broadening parameter was used for theoretical LDOS. The calculation is also limited, as detailed edge structure and possible defects in experimental samples are unknown, and edge relaxation and reconstruction are not counted. However, the agreement between several FM edges and the distinctive difference between FM and AFM edges as measured by experiments are all consistent with the calculated topological edge states, which makes it very unlikely that trivial (chemical) edge states would provide a sensible explanation, in addition to the consideration that the trivial band structures (Supplementary Figs 9–11) differ significantly from the ARPES data. We expect future transport measurement to be a very interesting experiment to further reveal the topological properties.

In conclusion, for the first time, we demonstrate the coexistence of topological and superconducting states in one material of single-layer FeSe/STO film, based on first-principles theory, STS and ARPES experiments. Our find provokes an exciting opportunity to study 2D topological superconductors through the proximity effect, which may help advance our fundamental

understanding of physical properties associated with the topological superconducting state, such as Majorana fermions, and pave the way to building novel quantum and spintronics devices by interfacing a superconductor with a topological insulator through a p–n junction since n- and p-type FeSe is respectively a superconductor and topological insulator.

Methods

Methods and any associated references are available in the online version of the paper.

Received 10 November 2014; accepted 27 May 2016; published online 4 July 2016

References

1. Wang, Q. *et al*. Interface-induced high-temperature superconductivity in single unit-cell FeSe Films on $SrTiO_3$. *Chin. Phys. Lett.* **29,** 037402 (2012).
2. Liu, D. *et al*. Electronic origin of high-temperature superconductivity in single-layer FeSe superconductor. *Nature Commun.* **3,** 931 (2012).
3. He, S. *et al*. Phase diagram and electronic indication of high-temperature superconductivity at 65 K in single-layer FeSe films. *Nature Mater.* **12,** 605–610 (2013).
4. Tan, S. *et al*. Interface-induced superconductivity and strain-dependent spin density waves in FeSe/$SrTiO_3$ thin films. *Nature Mater.* **12,** 634–640 (2013).
5. Lee, J. J. *et al*. Interfacial mode coupling as the origin of the enhancement of T_c in FeSe films on $SrTiO_3$. *Nature* **515,** 245–248 (2014).
6. Zhang, W. *et al*. Direct observation of high-temperature superconductivity in one-unit-cell FeSe films. *Chin. Phys. Lett.* **31,** 017401 (2014).
7. Ge, J.-F. *et al*. Superconductivity above 100 K in single-layer FeSe films on doped $SrTiO_3$. *Nature Mater.* **14,** 285–289 (2015).
8. Hao, N. & Hu, J. Topological phases in the single-layer FeSe. *Phys. Rev. X* **4,** 031053 (2014).
9. Wang, Z. *et al*. Topological nature of the $FeSe_{0.5}Te_{0.5}$ superconductor. *Phys. Rev. B* **92,** 115119 (2015).
10. Hao, N. & Shen, S.-Q. Topological superconducting states in monolayer FeSe/$SrTiO_3$. *Phys. Rev. B* **92,** 165104 (2015).
11. Coh, S., Cohen, M. L. & Louie, S. G. Large electron–phonon interactions from FeSe phonons in a monolayer. *New J. Phys.* **17,** 073027 (2015).
12. Liu, K., Lu, Z.-Y. & Xiang, T. Atomic and electronic structures of FeSe monolayer and bilayer thin films on $SrTiO_3$(001): first-principles study. *Phys. Rev. B* **85,** 235123 (2013).
13. Berlijn, T. *et al*. Doping effects of Se vacancies in monolayer FeSe. *Phys. Rev. B* **89,** 020501(R) (2014).
14. Bazhirov, T. & Cohen, M. L. Effects of charge doping and constrained magnetization on the electronic structure of an FeSe monolayer. *J. Phys. Condens. Mater.* **25,** 105506 (2013).
15. Zheng, F., Wang, Z., Kang, W. & Zhang, P. Antiferromagnetic FeSe monolayer on $SrTiO_3$: the charge doping and electric field effects. *Sci. Rep.* **3,** 2213 (2013).
16. Hor, Y. S. *et al*. Superconductivity in $Cu_xBi_2Se_3$ and its implications for pairing in the undoped topological insulator. *Phys. Rev. Lett.* **104,** 057001 (2010).
17. Novak, M. *et al*. Unusual nature of fully gapped superconductivity in In-doped SnTe. *Phys. Rev. B* **88,** 140502(R) (2013).
18. Kane, C. L. & Mele, E. J. Quantum spin Hall effect in graphene. *Phys. Rev. Lett.* **95,** 226801 (2005).
19. Wang, Z. F., Su, N. & Liu, F. Prediction of a two-dimensional organic topological insulator. *Nano Lett.* **13,** 2842–2845 (2013).
20. Bernevig, B. A., Hughes, T. L. & Zhang, S.-C. Quantum spin Hall effect and topological phase transition in HgTe quantum wells. *Science* **314,** 1757–1761 (2006).
21. König, M. *et al*. Quantum spin Hall insulator state in HgTe quantum wells. *Science* **318,** 766–770 (2007).
22. Mong, R. S. K., Essin, A. M. & Moore, J. E. Antiferromagnetic topological insulators. *Phys. Rev. B* **81,** 245209 (2010).
23. Essin, A. M. & Gurarie, V. Antiferromagnetic topological insulators in cold atomic gases. *Phys. Rev. B* **85,** 195116 (2012).
24. Guo, H., Feng, S. & Shen, S.-Q. Quantum spin Hall effect induced by nonmagnetic and magnetic staggered potentials. *Phys. Rev. B* **83,** 045114 (2011).
25. Mostofi, A. A. *et al*. Wannier90: a tool for obtaining maximally-localised Wannier functions. *Comput. Phys. Commun.* **178,** 685–699 (2008).
26. Wang, Z. F., Liu, Z. & Liu, F. Organic topological insulators in organometallic lattices. *Nature Commun.* **4,** 1471 (2013).
27. Wang, Z. F., Chen, L. & Liu, F. Tuning topological edge states of Bi (111) bilayer film by edge adsorption. *Nano Lett.* **14,** 2879–2883 (2014).
28. Yang, F. *et al*. Spatial and energy distribution of topological edge states in single Bi(111) bilayer. *Phys. Rev. Lett.* **109,** 016801 (2012).
29. Tamai, A. *et al*. Strong electron correlations in the normal state of the iron-based $FeSe_{0.42}Te_{0.58}$ superconductor observed by angle-resolved photoemission spectroscopy. *Phys. Rev. Lett.* **104,** 097002 (2010).
30. Maletz, J. *et al*. Unusual band renormalization in the simplest iron-based superconductor $FeSe_{1-x}$. *Phys. Rev. B* **89,** 220506(R) (2014).

Acknowledgements

Z.F.W. and F.Liu acknowledge financial support from DOE-BES (No. DE-FG02-04ER46148). Z.F.W. acknowledges additional financial support from the Chinese Youth 1000 Talents Program and Fundamental Research Funds for the Central Universities. X.J.Z. acknowledges financial support from the NSFC (No. 11190022 and 11334010) and the Strategic Priority Research Program (B) of CAS (No. XDB07020300). Q.K.X. and X.M. acknowledge financial support from the MOST of China (No. 2009CB929400 and 2012CB921702). We also thank the Supercomputing Center at USTC, NERSC and CHPC at University of Utah for providing the computing resources.

Author contributions

Z.F.W. and F.Liu conceived the project, and Z.F.W. carried out the theoretical calculation. H.Z., C.L., C.T., C.S., Y.Z., J.P., F.Li, C.N., L.W., X.M. and Q.K.X. carried out the MBE thin-film growth and STS measurement. D.L. and X.J.Z. carried out the ARPES measurement. Z.F.W. and F.Liu prepared the manuscript with input from X.J.Z., X.M. and Q.K.X.

Additional information

Supplementary information is available in the online version of the paper. Reprints and permissions information is available online at www.nature.com/reprints. Correspondence and requests for materials should be addressed to X.J.Z., X.M. or F.Liu.

Competing financial interests

The authors declare no competing financial interests.

Methods

Theoretical calculation. First-principles calculations, including SOC, were carried out in the framework of generalized gradient approximation with the Perdew–Burke–Ernzerhof functional using the Vienna Ab initio simulation package (VASP)[31]. The single-layer FeSe was adsorbed on the 1×1 unit cell of TiO_2-terminated 6-layer STO slabs. The in-plane lattice constant was fixed to the experimental value $a = 3.901$ Å (refs 1,15). All of the calculations were performed with a plane-wave cutoff of 400 eV on the $9 \times 9 \times 1$ Monkhorst–Pack k-point mesh. The vacuum layer was 15 Å thick to ensure decoupling between neighbouring slabs. During structural relaxation, all atoms were relaxed until the forces were smaller than 0.01 eV $Å^{-1}$. In addition, further increasing the thickness of the STO substrate will not change the FeSe band structures (Supplementary Fig. 19). We have chosen the default setting in VASP to add the on-site Coulomb interaction (LDAUTYPE = 2), and the U value is added to the *d* electron of Fe atoms.

FeSe/STO thin-film growth. The Nb-doped (001)-oriented single-crystal STO (Shinkosha, wt 0.5%) was chosen as the substrate for FeSe growth. The substrates were cleaned by ethanol and acetone before being transferred into the molecular beam epitaxy (MBE) chamber. After degassing at 550 °C for 8 h, Se flux treatment was performed to get smooth STO surfaces. FeSe films were grown by co-evaporating Fe (99.995%) and Se (99.9999%) from Knudsen cells with a flux ratio of more than 1:10 while keeping the substrate at 300 °C. The nominal growth rate was estimated to be about 0.075 ml min^{-1}. Then the FeSe film was gradually annealed up to 500 °C for one hour before taking the STS measurement. The prepared FeSe/STO films were capped by amorphous Se to protect the samples from the air when transferring the sample out of the MBE chamber into the ARPES measurement chamber[2,3]. The films were decapped by annealing at a temperature of about 450 °C for a few hours, under which the Se can be removed completely. This has been confirmed by STM and ARPES in more than one hundred samples. Meanwhile, the electronic structure of the samples is well understood through the annealing processes.

STM and STS measurement. The STM/STS experiments were conducted in a Unisoku ultrahigh-vacuum low-temperature STM system interconnected to a MBE chamber for film preparation. The base pressure is better than 2×10^{-10} torr. All of the data were acquired at 4.3 K. A polycrystalline Pt–Ir tip was used for STM/STS investigation, and calibrated on a MBE-grown Ag film on a Si(111) substrate. All differential conductance dI/dV spectra were acquired using a standard lock-in technique at 966 Hz.

ARPES measurement. High-resolution ARPES measurements were carried out on our laboratory system equipped with a Scienta R4000 electron energy analyser and with a base pressure better than 5×10^{-11} torr (refs 2,3). We used a helium discharge lamp as the light source, which can provide photon energies of $h\nu = 21.218$ eV. The energy and angular resolutions were 4–10 meV and 0.3°, respectively.

References

31. Kresse, G. & Hafner, J. *Ab initio* molecular dynamics for liquid metals. *Phys. Rev. B* **47,** 558–561(R) (1993).